On the Expected Structure of Extreme Waves in a Gaussian Sea. Part II: SWADE Scanning Radar Altimeter Measurements

O. M. PHILLIPS AND DAIFANG GU

Earth and Planetary Sciences, The Johns Hopkins University, Baltimore, Maryland

EDWARD J. WALSH

NASA Goddard Space Flight Center, Greenbelt, Maryland

16 November 1992 and 1 April 1993

ABSTRACT

In a previous paper (Phillips et al.) an approximate theory was developed that predicted that the expected configuration of extreme waves in a random sea (or the average configuration of an ensemble of extreme waves) is proportional to the space–time autocorrelation function of the surface displacement of the wave field as a whole. This result is tested by examination of scanning radar altimeter measurements made during SWADE in four different sea states, including a unimodal mature wave field, a short fetch, a wind-generated sea crossing swell, a very broad directional spectrum, and a fetch-limited wind sea with opposing swell. In each of these, the spatial autocorrelation function was found directly from the SRA data. The highest waves in each dataset were selected and their configurations averaged with respect to the crest. These averaged configurations were in each case found to be consistent with the autocorrelation function.

1. Introduction

The question of the expected configuration in space and time of the sea surface in the vicinity of extreme wave crests and its dependence on the wavenumber frequency spectrum is an important one in naval architecture. The design of ships and structures capable of withstanding encounters with these events would be aided by a knowledge of not only the probability of occurrence of a wave of extreme height but also the expected shape of the wave near such a crest. The expected configuration is, equivalently, the mean configuration averaged over an ensemble of extreme events in a given sea condition; in a random sea one cannot predict when or where the extreme crests will occur but one can predict what their expected configuration will be when they do occur.

Even if one assumes that the wave field is Gaussian, the calculation of the expected surface displacement $\bar{\zeta}(\mathbf{x}+\mathbf{r}, t+\tau)$, given that at $(\mathbf{x}, t)$, ζ has a maximum ζ_m that is a substantial multiple of the rms value $\sigma = (\bar{\zeta}^2)^{1/2}$, though direct in principle, is extraordinarily cumbersome to perform analytically, and it has not in fact been done. The corresponding direct calculation of $\bar{\zeta}(t)$ surrounding high maxima in a simple time series is reasonably tractable when the spectrum is narrow (as specified by Longuet-Higgins 1984); the details were given in a previous paper (Phillips et al. 1993) and compared with buoy measurements obtained during the Surface Wave Dynamics Experiment (SWADE) in the October 1990 storm.

The full three-dimensional $(\mathbf{x}, t)$ calculation is so cumbersome because it involves conditional probabilities not only on the largeness of $\zeta(\mathbf{x}, t)$ but also multiple conditions on its space and time derivatives. In view of this, a much simpler approximate theory was developed in which the question is asked in a slightly different way. Rather than seeking the precise points where ζ attain maxima, let us consider those *regions* in space and time where $\zeta \geqslant \gamma\sigma$, where γ is (formally) a number large compared with unity. For a given γ, these regions consist of isolated islands containing at least one maximum, and as γ increases, the islands shrink, converging toward the maxima and then disappearing. Our interest is in large values of γ, where there are rare, small, isolated islands in which $\zeta \geqslant \gamma\sigma$; let us ask this question: Given that at $(\mathbf{x}, t)$, say, $\zeta \geqslant \gamma\sigma$ where γ is large, what is the expected distribution or configuration of $\zeta(\mathbf{x}+\mathbf{r}, t+\tau)$ in the vicinity and what is the expected standard deviation about it? This is a much simpler calculation (which makes sense only when γ is large), and it was shown in the previous paper that

Corresponding author address: Dr. Owen M. Phillips, Department of Earth and Planetary Sciences, Olin Hall, 3400 N. Charles Street, The Johns Hopkins University, Baltimore, MD 21218.

$$\bar{\zeta}(\mathbf{x}+\mathbf{r}, t+\tau) = \bar{\zeta}(\mathbf{x}, t)_{\zeta>\gamma\sigma} \cdot \rho(\mathbf{r}, \tau), \quad (1.1)$$

where $\rho(\mathbf{r}, \tau)$ is the space–time autocorrelation function for the entire wave field:

$$\rho(\mathbf{r}, \tau) = \overline{\zeta(\mathbf{x}, t)\zeta(\mathbf{x}+\mathbf{r}, t+\tau)} / \overline{\zeta^2}. \quad (1.2)$$

In an ensemble of extreme wave crests, in the vicinity of the crests, the variance about the mean (1.1) is small, approximately $\gamma^{-2}\sigma^2$, but increases as the envelope of the correlation function decreases, approaching σ^2 as $\bar{\zeta}(\mathbf{x}+\mathbf{r}, t+\tau) \to 0$.

In this paper, we will examine data on the spatial structure of extreme waves to test the usefulness of the approximate result (1.1). Some information on the spatial structure and propagation of groups of large waves has been obtained by Boccotti et al. (1993) with an array of nine wave gauges arranged in two rows in water 3–4 m deep off the Reggio Calabria beach on the Straits of Messina. However, more extensive measurements of the spatial structure of wind-generated waves are now becoming available in the scanning radar altimeter (SRA) observations obtained during the intensive observation periods of SWADE in March 1991.

The SRA is a mode of the NASA/Goddard Space Flight Center Multimode Airborne Radar Altimeter (Parsons and Walsh 1989). It is a 36-GHz, computer-controlled pulse radar that produces a *real-time* topographical map of the surface beneath the aircraft on which it is carried. This system supersedes the surface contour radar described by Kenney et al. (1979), which was used for measurements of directional wave spectra by Walsh and his colleagues (1985a, 1991). In brief, a rotating mirror scans the SRA 1.0° half-power width (two-way) pencil beam laterally through ±22° to measure the slant range to 64 evenly spaced points on the surface below the aircraft. Corrections are made in real time for the off-nadir angle of the beam (including the roll attitude of the aircraft). The spacing between points sampled in a cross-track traverse is proportional to the aircraft altitude; in the results from SWADE to be discussed here, it varied between 2.1 m in case 4A, 13.3 m in case 5A, and about 8 m in cases 5B and 5C. The spacing alongtrack between the lateral traverses is proportional to the aircraft speed and in these measurements was between 12 and 14.2 m. Sea surface displacements were quantized to the nearest 10 cm. Since it involves a direct range measurement, the SRA provides, in principle, one of the most straightforward remote sensing instruments. If every single return pulse were sharp and cleanly detected, the two-dimensional surface along the swath would be unambiguously defined at these scales of resolution; in practice a certain fraction of the return signals is too weak to be detected

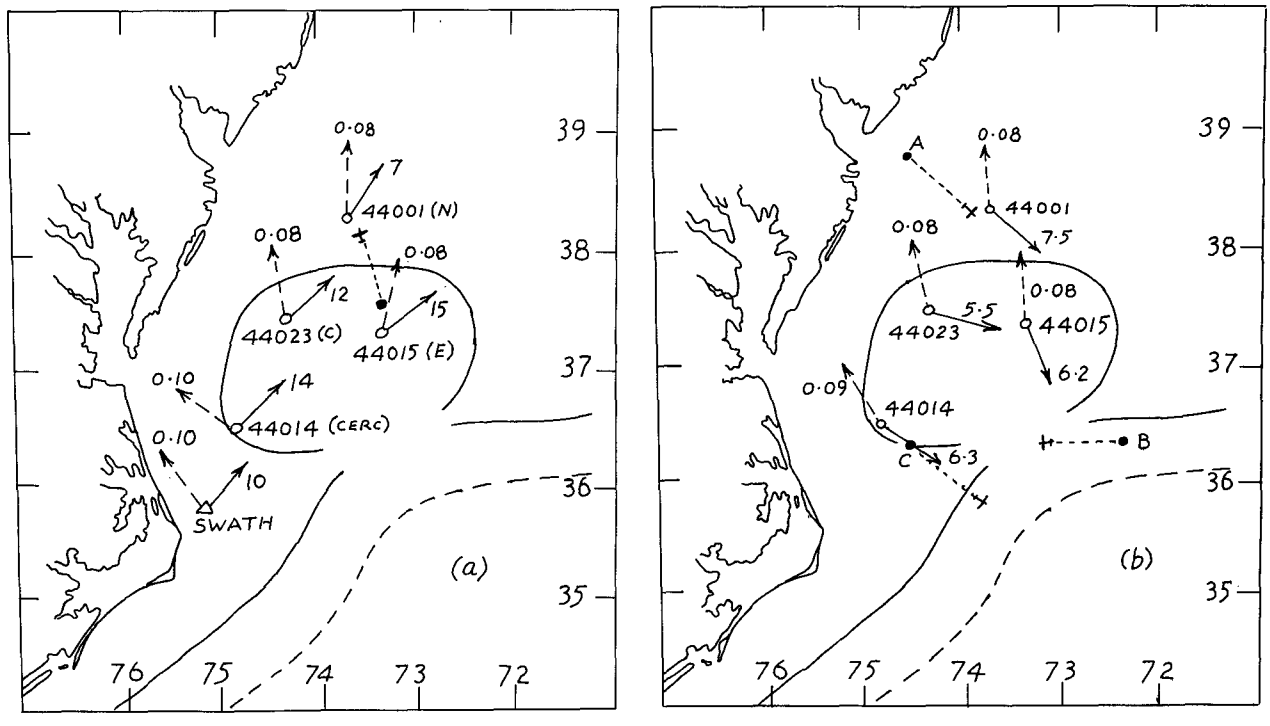

FIG. 1. The SWADE measurement area. Open circles indicate NDBC buoys with wind speeds (m s^{-1}) and directions indicated by the solid arrows, dominant swell frequency (Hz), and direction by the broken arrows. Measurement points and flight paths are indicated by solid dots. The inner and outer approximate edges of the Gulf Stream are shown by the solid and broken curves, with a detaching warm eddy to the north. Panel (a) represents conditions at about 2230 UTC 4 March 1991, and panel (b) during 1700–2000 UTC 5 March.

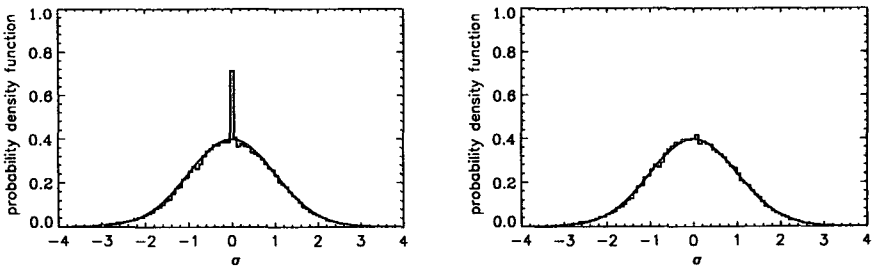

FIG. 2. A typical distribution of ζ before and after correction for spurious zeros.

or too ragged to be timed precisely, and this provides a noise problem that must be identified and coped with. Our procedure for doing this is described in detail in the following.

2. The SWADE SRA data samples

In this paper, we use SRA data swaths obtained under several different wind-generation conditions (a) to extract the spatial autocorrelation function $\overline{\zeta(\mathbf{x})\zeta(\mathbf{x}+\mathbf{r})}/\overline{\zeta^2}$ for the wave field as a whole; (b) to search for the highest wave crests (maxima above mean water level) to form small ensembles of realizations of the sea surface surrounding these crests, from which the mean configuration in the vicinity can be found; and (c) to compare the shapes of these two surfaces in order to test the usefulness of (1.1).

The SWADE intensive measurement area was in the general region from 35° to 39°N and from the U.S. eastern seaboard to about 72°W—from Cape Hatteras to the mouth of the Delaware River and up to about 300 km offshore. The first of the datasets we have examined was acquired at 1730 LST (2230 UTC) on the afternoon of 4 March 1991 in the vicinity of 37.6°N, 73.3°W, not far from The National Data Buoy Center (NDBC) meteorological buoy 44015 (Discus E—see Fig. 1). During the previous 3 days, the wind had been generally from the south over the midcontinental seaboard, and for 7 h prior to the measurement, the wind over the area had been backing from the southwest toward the west (from 220° to 250°), with speeds measured at discus E, central, and CERC decreasing from 13–15 m s^{-1} to about 4–8 m s^{-1}. The significant wave height at Discus E was 5.5 m at 2200 UTC with a dominant period of 12.5 s. The air temperature was 16.7°, and the water temperature 20.4°. Velocity and temperature measurements by Shay (1993), taken the following day, indicate the presence of a detaching warm eddy north of the Gulf Stream, with near-surface currents of less than 1 m s^{-1}. During the following night, a cold-air outbreak occurred with winds now blowing offshore from the northwest. Three further segments of data were acquired between 1700 and 2000 UTC 5 March when the wind speed over the previous 6 h had ranged from 7 to 9 m s^{-1} over the area, and direction from 290° to 335°. The air temperatures were from 7° to 10°C at the three more southerly buoys and from 5° to 6°C at Discus N; the temperature front of the Gulf Stream was still west of the three southerly buoys while south of Discus N. Data were acquired at the three locations, 5A, 5B, and 5C, shown in Fig. 1. The first of these was close inshore (38.74°N, 74.55°W)

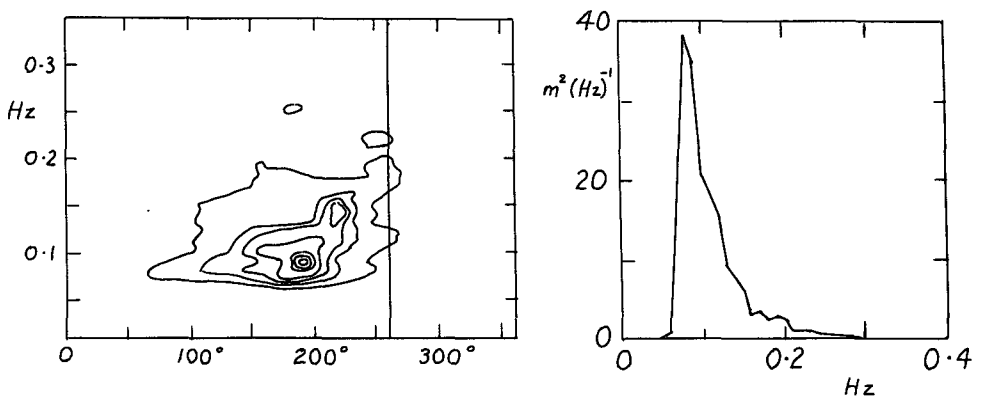

FIG. 3. Directional-frequency spectrum and frequency spectrum at buoy 44015 (Discus E) at 2200 UTC 4 March. In this and subsequent figures, the directions are those *from* which the waves are propagating. Contours represent 0.01, 0.05, 0.1, 0.2, 0.4, 0.6, and 0.8 of the peak.

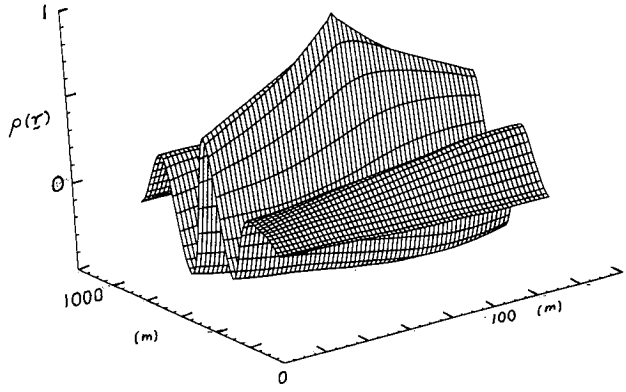

FIG. 4. The spatial autocorrelation function for the wave field, calculated from the entire SRA swath of 4 March.

off the mouth of the Delaware Bay; the significant wave heights were relatively small (1.55 m) and the spectrum of waves turned out to be relatively simple. The set 5B was obtained in the main Gulf Stream near 36.37°N, 72.40°W, where the near-surface currents measured by Shay (1993) were about 2 m s^{-1} to the east. The wave field here was expected to have been influenced by refraction as it entered the stream. The final set, 5C, was taken near 36.30°N, 74.60°W, near the southwestern edge of the warm eddy, with a significant wave height of about 2 m and, as subsequently appeared, a double spectral peak.

Each of the datasets examined contained 1530 lateral traverses, each of 64 points—a matrix of 64 columns and 1530 rows. The first step was to examine the cross-track homogeneity of the data to detect any biases associated with incidence angle. It quickly became apparent that in data obtained at higher altitudes (1050 m for 5A and 640 m for 5B, C) the six columns on each side were quite unreliable, and the mean-square fluctuations reported were substantially higher toward the sides than they were near the center, close to nadir [see Walsh et al. (1985b) for discussion]. The center 24 columns varied little ($\pm c$ 10%) in their mean squares, so that the matrix for analysis was reduced to 24 × 1530, a total of 36 720 points for these sets. In the low-altitude flight (4A at 168 m) the center 51 columns were acceptable, with a total of 78 030 points.

The second step was to go through the printouts of the data in detail, looking for dropouts, indicated by

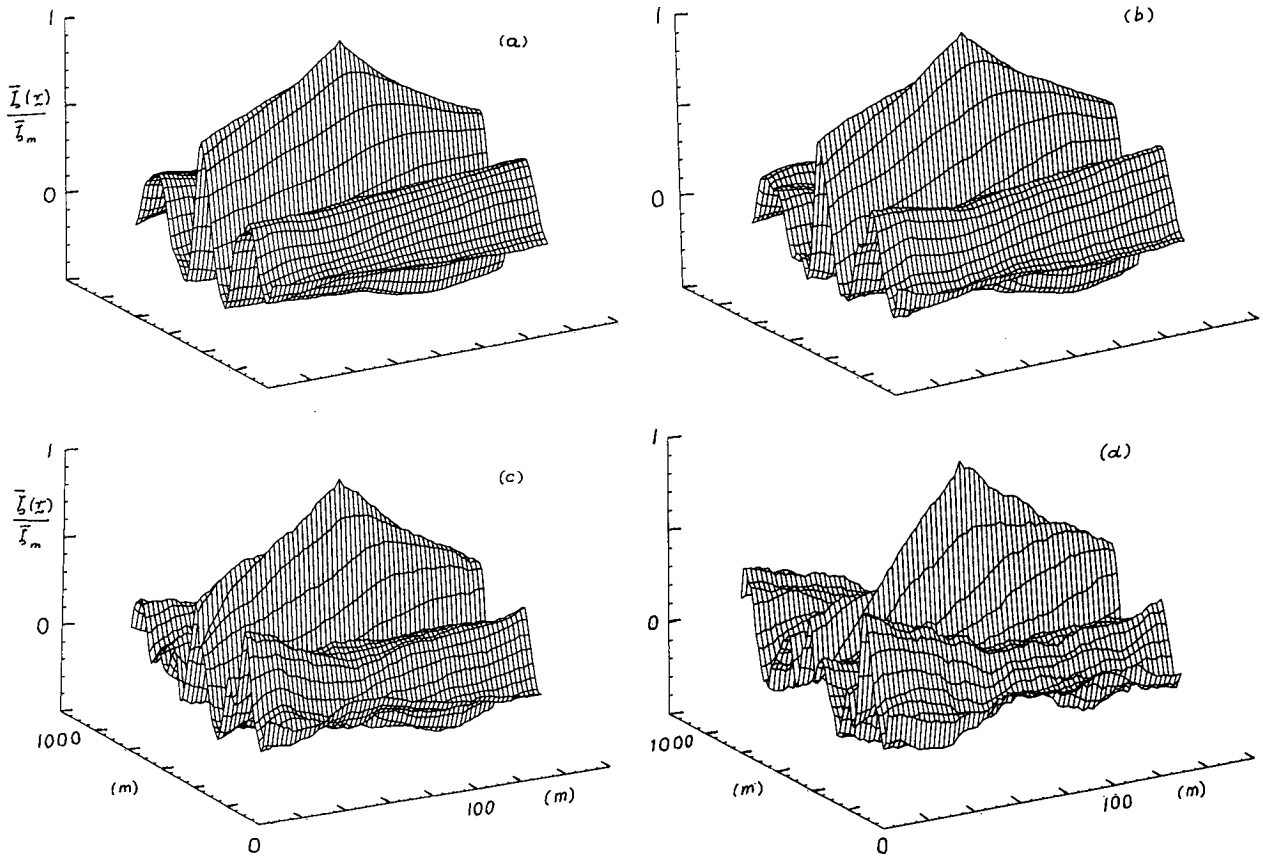

FIG. 5. Mean surface configurations surrounding high crests in the data used in Fig. 4: (a) mean for crests higher than 2σ, (b) 2.5σ, (c) 3σ, and (d) 3.5σ.

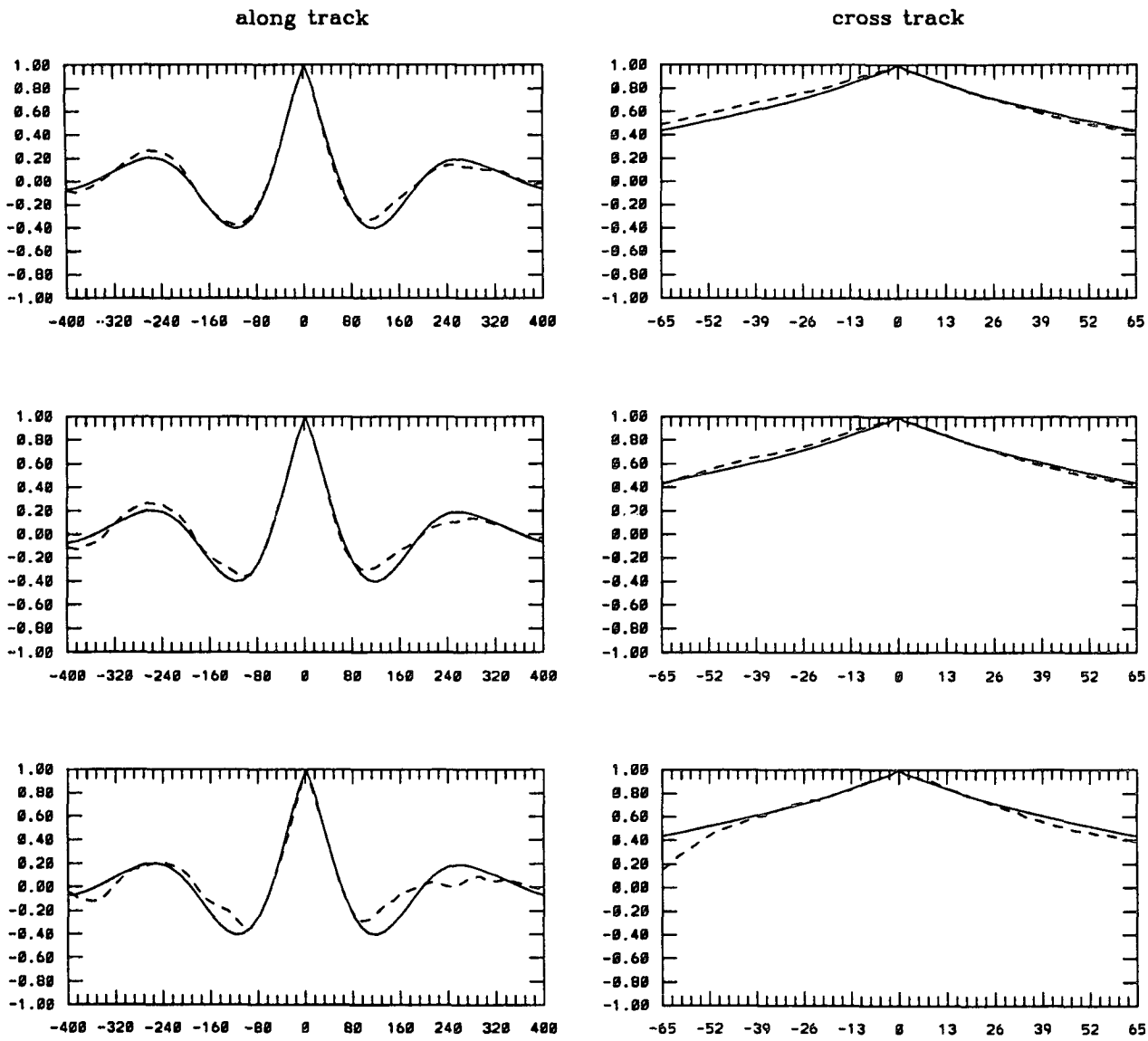

FIG. 6. Sections of mean configurations of Fig. 5 along and across track for γ = 2.0, 2.5, and 3.0 (dashed lines) compared with corresponding sections of the autocorrelation function.

the symbol "−99," or rows in which the instruments failed to record, identified by "−88." Real data generally lay within the range ±50 in units of 0.1 m. Rows of missing data (a percent or so of the total) occurred singly and were replaced by values linearly interpolated alongtrack. When individual return pulses were not strong enough to be picked up by the radar, "−99" was supposed to be recorded. These were randomly distributed throughout the matrix, mostly isolated but sometimes in small clusters. Wherever possible, these values were filled in by interpolation between adjacent points; when missing points were grouped, diagonal interpolations were used. Only a few clusters of missing data remained after this procedure and they were replaced by averages using whatever available adjacent points there were.

Next, the probability density functions of the values in each dataset, digitized at intervals of 0.1 m, were examined, and Fig. 2 shows a typical result. The distribution should of course be closely Gaussian, with a possible excess of very large values and a deficit of very small ones, but it is immediately apparent that the data contain a significant number of spurious zeros. The fraction of these was estimated by subtracting from the number recorded the number to be expected in the data with this digitizing interval and the appropriate

rms. It is not entirely clear why the spurious zeros were recorded—of the data of set 4, 2.5% were spurious zeros, of set 5A, 7.2%, of set 5B, 6.4% and of set 5C, 9.9%. Apparently, some trap in the standard data processing was inadvertently setting some class of outlier to zero instead of −99. Nor was it possible to identify with any certainty which individual values of zero were real and which were spurious, but it is possible to correct the autocorrelation function, calculated from the data, for their presence.

If one assumes that they are distributed randomly throughout the data, then in calculating $\overline{\zeta^2}$, a fraction q of the values in the summation is spuriously zero, so that the mean found $(\overline{\zeta^2})_q$ is $(1 - q)\overline{\zeta^2}$. Accordingly, the true value

$$\sigma^2 = \overline{\zeta^2} = (1 - q)^{-1}(\overline{\zeta^2})_q. \tag{2.1}$$

In the calculation of the covariances for fixed $\mathbf{r} \neq 0$, $\overline{\zeta(\mathbf{x})\zeta(\mathbf{x} + \mathbf{r})} = \overline{\zeta\zeta'}$, say, of the products of numbers that are summed, the first factor is a spurious zero in

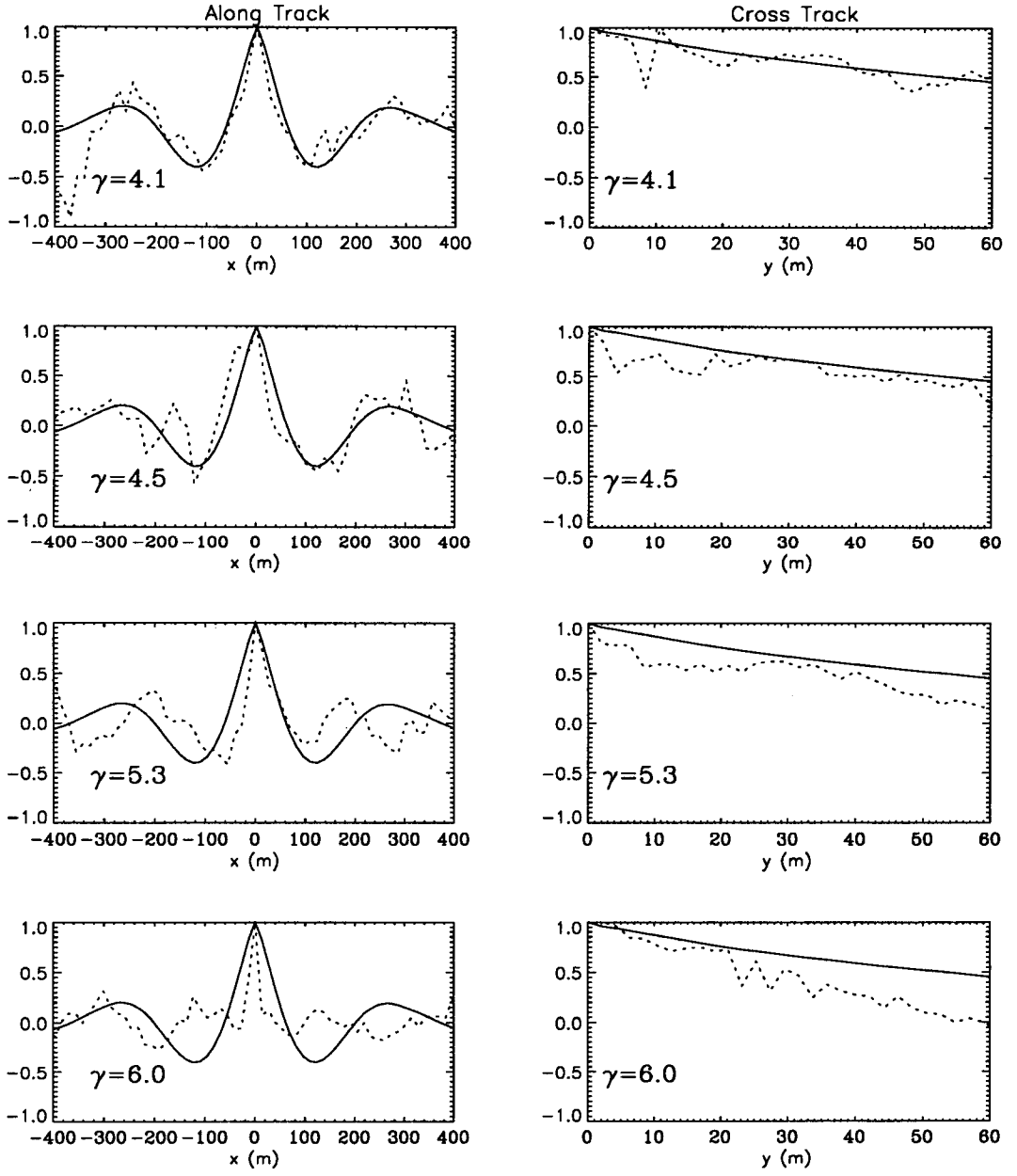

FIG. 7. Alongtrack and across-track sections of the highest individual crests. The lowest one is almost certainly spurious.

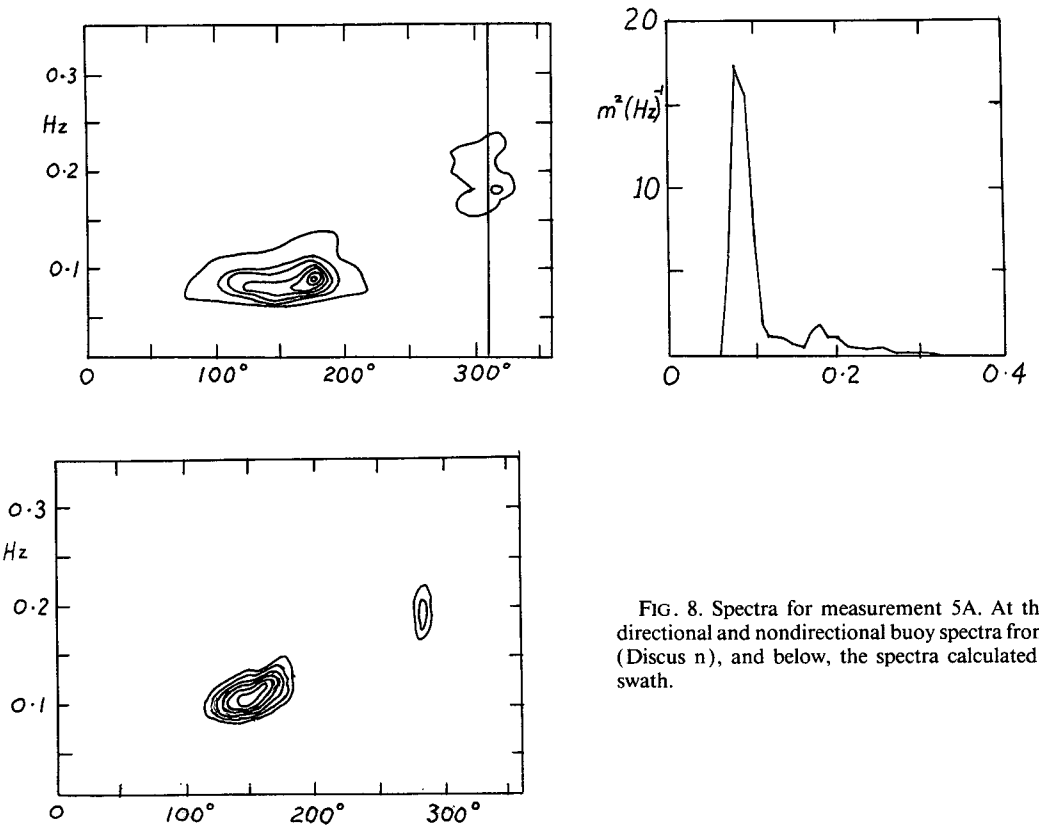

FIG. 8. Spectra for measurement 5A. At the top are the directional and nondirectional buoy spectra from buoy 44001 (Discus n), and below, the spectra calculated for the SRA swath.

the fraction q of them, as also in the second. This includes the fraction q^2 when both factors are spurious zeros, so that the resultant mean $(\overline{\zeta\zeta'})_q$ is too small by the fraction $2q - q^2$. Accordingly,

$$(\overline{\zeta\zeta'})_q = (1 - 2q + q^2)\overline{\zeta\zeta'}.$$

and

$$\overline{\zeta\zeta'} = (1 - q)^{-2}(\overline{\zeta\zeta'})_q \quad \text{when} \quad \mathbf{r} \neq 0, \quad (2.2)$$

so that the autocorrelation function

$$\rho(\mathbf{r}) = \overline{\zeta\zeta'}/\overline{\zeta^2} = \begin{cases} (1 - q)^{-1}(\overline{\zeta\zeta'})_q/(\overline{\zeta^2})_q, & \mathbf{r} \neq 0, \\ 1, & \mathbf{r} = 0. \end{cases} \quad (2.3)$$

Another source of noise in the data arose from the sometimes ragged return signals from the surface, particularly at the relatively large incidence angles at off-nadir points where the surface sloped downward from the track axis. The raggedness in the signal made it difficult to determine the precise arrival time and therefore the value of the surface elevation, though individual erroneous points did not appear to influence strongly our estimates of the covariances or of averaged wave configurations, at least when the number of realizations was sufficiently large. In an examination of individual realizations, however, the possible presence of this noise demands that a critical eye be used, alert to the possibility that apparently very high values of ζ, used to pick out an extreme wave, may in fact be a noisy value. A couple of probable examples are described in section 3.

3. The configurations of extreme waves

a. A unimodal, mature wave field

The first set of results to be presented was obtained at 2230 UTC 4 March 1991, as mentioned earlier. The wind field had been uniform from the south over the previous 3 days but had begun to turn more from the southwest during the 7 h prior to the measurements. Figure 1a identifies the measurement region as the solid point with the flight track toward 345°. The locations of four neighboring buoys operated by the NDBC during SWADE are indicated by the open circles, with the average wind speed and direction over the previous 6 h shown by the solid arrows. The directions of the dominant waves at 2230 UTC are indicated by the broken arrows, and the attached figures give their frequencies in hertz. The SWATH (Small Waterplane Area Twin Hull) ship *Frederic G. Creed,* equipped with a directional wave array, was at 2013 UTC at the inshore location indicated by the triangle, and the wind

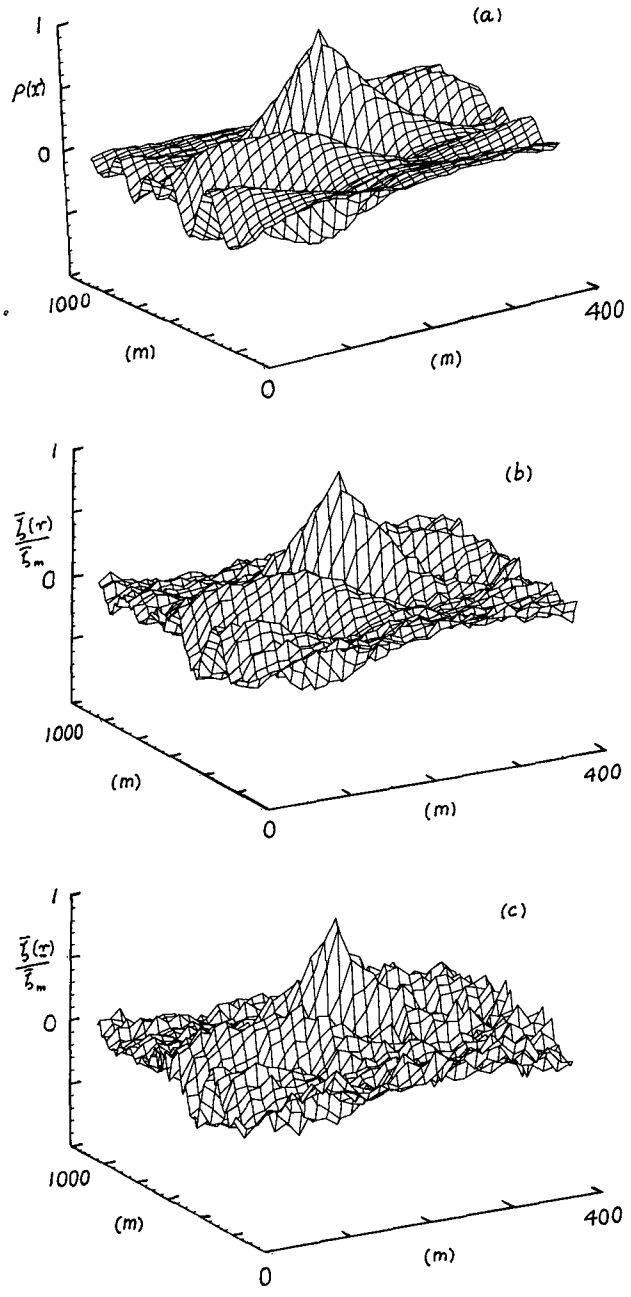

FIG. 9. Measurements from dataset 5A: (a) the spatial autocorrelation function and mean surface configurations surrounding crests, (b) higher than 2σ, and (c) higher than 2.5σ.

and wave characteristics there were similar to those measured by the buoy (44014, CERC) 70 km north-northwest.

The sharp inner edge of the Gulf Stream, marked in sea surface temperature imagery by an abrupt temperature change, is shown as the solid curve and the approximate outer edge of the current by the broken one. During these observations, the warm eddy was unusually close inshore, running close to the shelf break off Virginia. Waves of period 10–12 sec, propagating to the north, would be incident approximately normally to the upper, eastward flowing leg of the Gulf Stream and thus were influenced little by refraction, as the observations at 44014 and 44015 (Discuses N and E) indicate. Waves at glancing incidence are, however, refracted strongly by a current—for a maximum speed of 2 m s^{-1}, 10-sec waves are totally reflected by shear if the angle of incidence with the current is greater than about 60° (Phillips 1981). The wave directions measured at 44014 and by the *Frederic G. Creed,* both near the inner edge of the Gulf Stream as it flows north, are about 45° to the west of those measured elsewhere and seem consistent with refraction by the current. (Diffraction around the banks off Cape Hatteras may also contribute to the directionality measured by the *Creed* but probably not that at CERC.)

The SRA measurements were made about 25 km north of buoy 44015 (Discus E). Directional wave spectra were measured at the buoy, whose characteristics, and the data processing techniques used, are described by Steele et al. (1992). The spectrum for 2000 UTC computed from the first five directional Fourier components by the maximum entropy method and kindly supplied by K. Steele and D. Wang is shown in Fig. 3, with a spectral peak indicating dominant waves of period about 12 s propagating from 190° with less energetic, higher frequency waves aligned more closely to the wind. The frequency spectrum based on the buoy measurements and given by Donelan and Drennan (1992) is also shown; it has the canonical unimodal form, with a significant wave height of 5.6 m and a wave age c_d/U approaching unity. In spite of the presence of the Gulf Stream, then, the wave field at this location and this time appears close to a standard mature, unimodal state.

The flight path for the SRA measurements was toward 345° at an altitude of 168 m. The measured spatial autocorrelation function for surface displacement along the swath, corrected for spurious zeros, is shown in Fig. 4. In general, the overall configuration of an autocorrelation function reflects the larger-scale structures in a field (small-scale structures lose correlation rapidly), and the form of Fig. 4 indicates a field of moderately long-crested waves with a dominant wavelength of approximately 250 m, traveling slightly to the right of the flight path. This is consistent with the measurements at Discus E (44015). The discontinuity in slope at $\mathbf{r} = 0$ can be interpreted as a consequence of an "equilibrium range" spectral asymptote of k^{-4} or $k^{-3.5}$ in the wavenumber spectrum for scales larger than the sampling intervals (2.1 m across track and 14.2 m along).

The principal objective of this paper is to compare the spatial autocorrelation functions with the mean surface displacements at points surrounding high

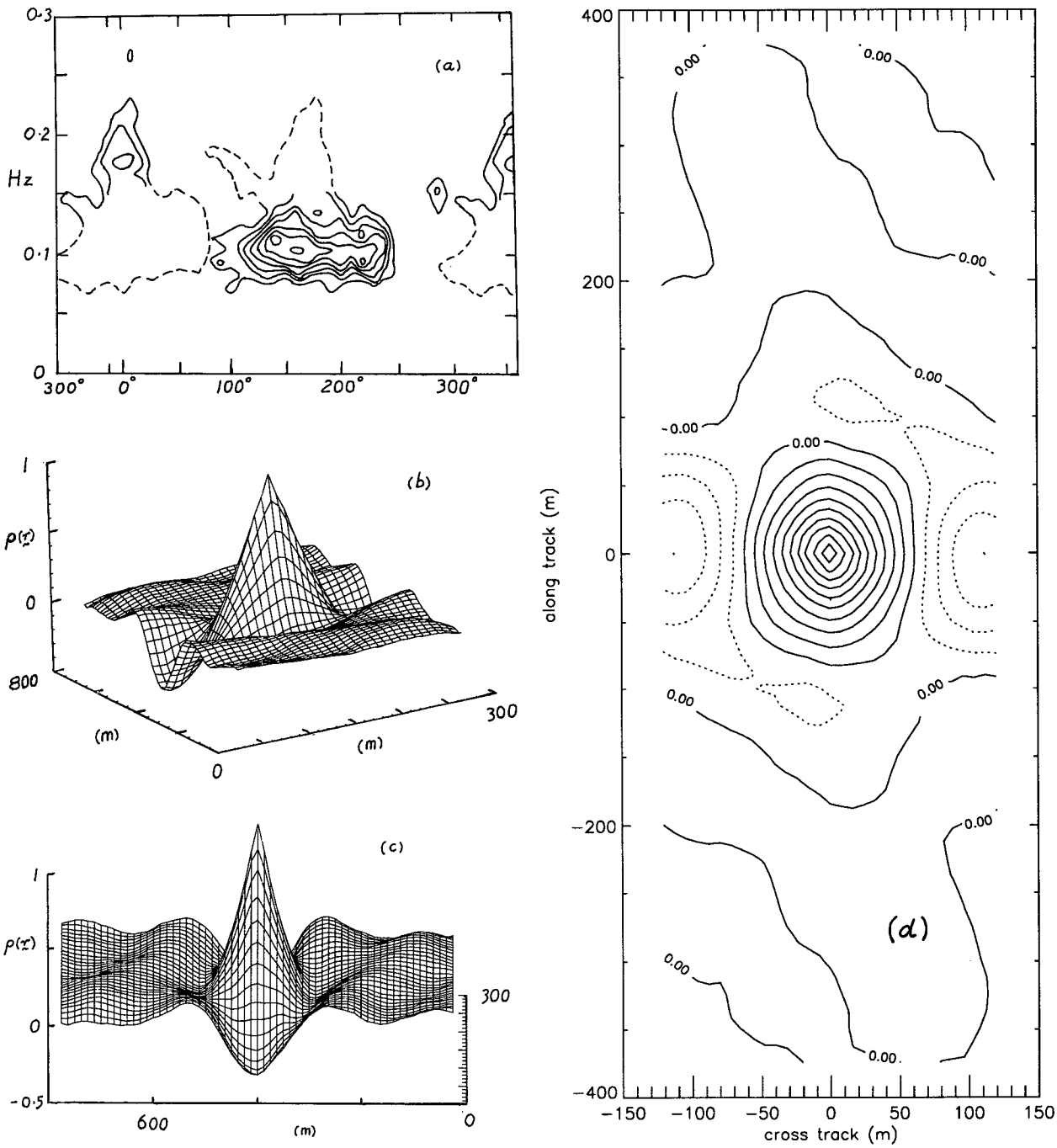

FIG. 10. The autocorrelation function for dataset 5B: (a) the SRA directional frequency spectrum; the autocorrelation function (b) looking downtrack from 30°, (c) looking cross track toward the north; and (d) contours with equal scales along and across track.

maxima in order to test the theoretical result (1.1). Accordingly, the data were scanned to identify points at which $\zeta > \gamma\sigma$ for given values of γ, and ensemble averages were taken of the surface displacements a distance **r** from the high points identified. The results are shown in Fig. 5 for $\gamma = 2$, 2.5, 3, and 3.5, the number of crests in each category being 389, 147, 50, and 17, respectively. For $\gamma = 2$, the average wave configuration is astonishingly (to us) similar to the spatial autocorrelation function of Fig. 4; the relation (1.1) was established only for large values of γ. As γ increases (Figs. 5b–d), the theory becomes better but the statistics be-

come worse since many fewer realizations are involved. Nevertheless, the primary characteristics of the configurations are preserved. The irregularity of Fig. 5d, in particular, is a consequence not primarily of noise but of the random wave field in which the high maxima are embedded and the small number of events in a record of finite size.

The quantitative differences between the autocorrelation function and the average configurations of the highest waves can be seen a little more clearly by superimposing sections of Fig. 5 along and across track. These are shown in Fig. 6 for γ = 2.0, 2.5, and 3.0; the agreement is close in the vicinity of the crest but deteriorates somewhat with increasing distance from the crest.

To obtain some sense of the variability of the extreme configurations, the four highest realizations were selected from the data, and normalized longitudinal and transverse sections from the crest are shown in Fig. 7 as the dotted lines. Corresponding sections of the autocorrelation function are also shown. The profiles with γ = 4.1 and 4.5 appear to be well consistent with the theory, since the random fluctuations of the measured configurations general lie within $\pm\sigma$ (0.22 to 0.25) of the expected ones. The case γ = 5.3 is somewhat doubtful; the central high point may be noisy. The case γ = 6 is almost certainly spurious. The prior probability of encountering such a high wave in a dataset of this size is miniscule ($<10^{-4}$), and in the alongtrack traverse, the high values are found in only one cross-track sweep, with values close to zero on either side. We do not regard this as credible.

b. A short-fetch wind-generated sea crossing swell (5A)

On 5 March, during the cold-air outbreak, winds were offshore from the northwest. The general situation during the 3-h period (1700–2000 UTC) over which the SRA measurements were made is illustrated in Fig. 1b. The local winds were generally from the northwest, generating a fetch-limited wind sea superimposed on the still-dominant lower frequency swell from the south. The first SRA swath (5A) was taken near the point A seaward of the mouth of Delaware Bay; the nearest buoy measurements were at Discus N (44001) some 80 km downwind. The directional frequency spectrum and the simple frequency spectrum there are

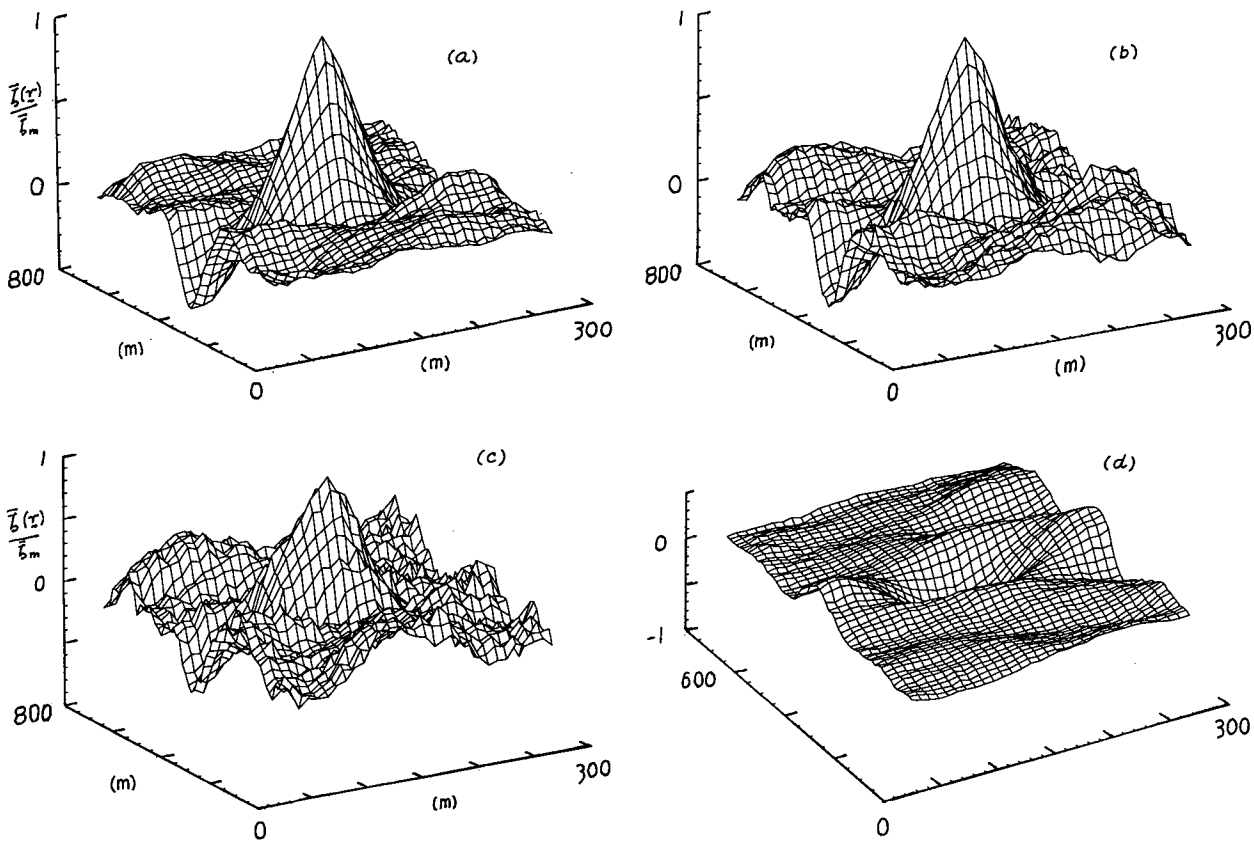

FIG. 11. Mean surface configurations surrounding high crests in the dataset 5B: (a) higher than 2σ, (b) 2.5, and (c) 3σ, and (d) surrounding troughs deeper than 2σ.

shown in Fig. 8, together with the directional spectrum at A computed from the SRA data with the use of the linear dispersion relation. The two types of directional spectrum have their separate characteristics. The angular distributions of buoy spectra at each frequency are derived from the amplitudes and phases (i.e., propagation direction) of the lowest two Fourier modes at each frequency and so may be directionally broader than the "true" spectra. The resolution in SRA spectra is much better along than across track, and the spectra have an intrinsic 180° ambiguity in the direction of wave propagation. Walsh et al. (1985) discuss how this can be resolved internally; with the supplementary information available during SWADE, the solution is usually obvious. Nevertheless, the two directional spectra of Fig. 8 are mutually supportive. Each shows a relatively small wind sea with a dominant frequency of about 0.18 Hz coming from 300° superimposed on a dominant low-frequency swell from the south. It is recorded at the buoy with a peak frequency of 0.08 Hz from 180° and by the SRA with a peak frequency of 0.10 Hz from 150°, possibly indicating refraction effects. The significant wave height was measured as 3.19 m at the buoy, and 2.1 m along the SRA swath, closer inshore.

The autocorrelation function of the waves in the SRA data is shown in Fig. 9a. Looking downwind, one identifies the dominant swell coming from a direction to the right of the swath, as illustrated in Fig. 1b. The wind sea, moving along the swath with about one-quarter the wavelength of the swell, is perhaps less evident, though the sharpness of the peak at the origin is indicative of smaller-scale waves. Also, the highest individual wave crests are likely to be those in the swath in which the swell crests and wind-sea crests happen to coincide, and the same characteristics are seen in the mean surface shapes surrounding high crests for $\gamma = 2$ (313 events) shown in Fig. 9b. The large-scale structure is again very similar to that of the autocorrelation function. When $\gamma = 2.5$ (97 events), the signal-to-noise level is clearly much smaller (the digitization internal is as much as 0.2σ in these relatively small waves), and even the general features are hard to discern.

c. *A very broad directional spectrum (5B)*

Point B was about 400 km offshore, south and east of the Gulf Stream, and SRA data were obtained here about 3 h later than at point A. Unfortunately, there were no pitch–roll buoys in the vicinity to provide a comparison with the spectrum calculated from the SRA data, which is shown in Fig. 10a. The 180° ambiguity in this instance is more difficult to resolve. The low-frequency swell must be coming generally from the south and east of south, though swell incident from the south on the Gulf Stream off Cape Hatteras would be refracted easterly toward the observation site. The

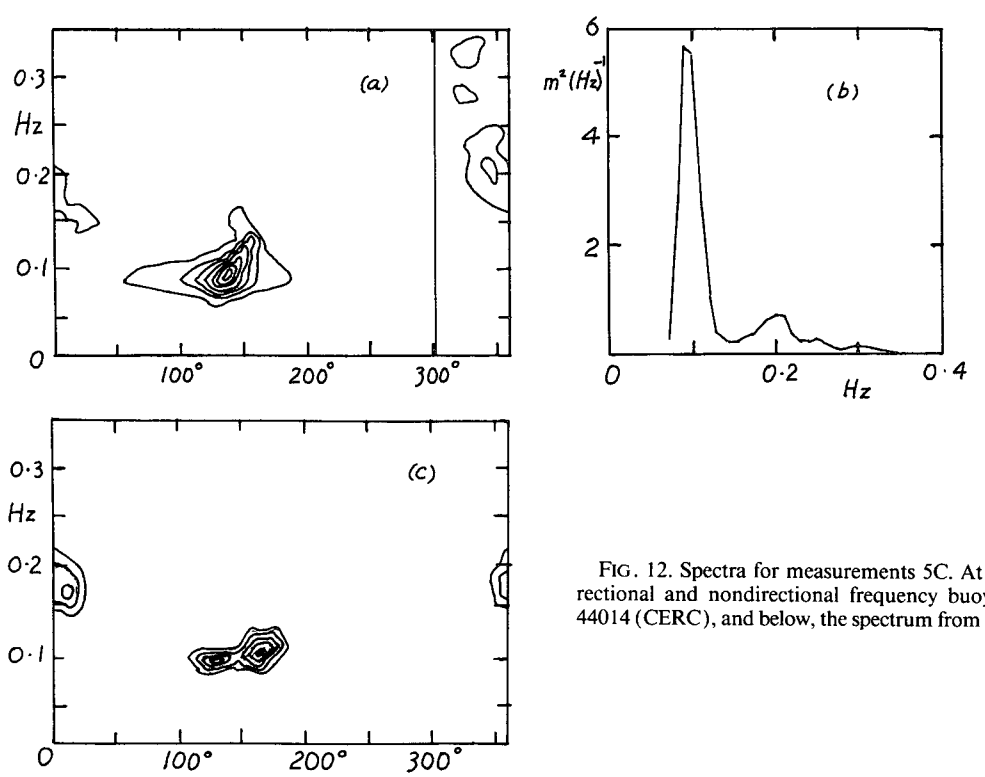

FIG. 12. Spectra for measurements 5C. At the top are directional and nondirectional frequency buoy spectra from 44014 (CERC), and below, the spectrum from the SRA swath.

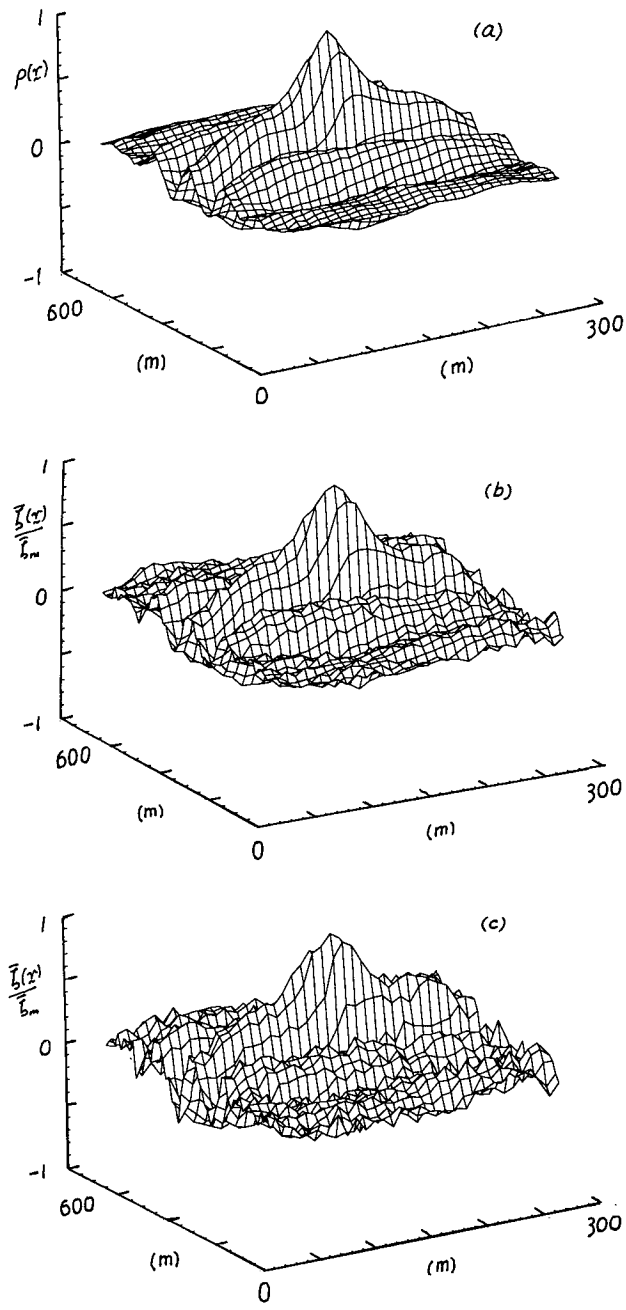

FIG. 13. (a) The spatial autocorrelation function for dataset 5C; mean surface configurations surrounding crests (b) higher than 2σ and (c) higher than 2.5σ.

wind sea generated off the coast and propagating through the warm eddy would arrive at site B from north to northwest; in Fig. 10a the two wave fields merge because of the ambiguity, but the division between them was taken, somewhat arbitrarily, at 0.15 Hz. Be that as it may, it is clear that the low-frequency swell, with a maxima at frequencies near 0.1 Hz, has an extremely wide directional spread, with a relatively flat distribution of spectral density at 0.1 Hz between 120° and 230°. Fetch-limited 6-sec waves from the north-northwest combined with the 10-sec swell from a wide arc from the south produced what must have been an extremely confused sea state, with a significant wave height of 3.2 m.

The autocorrelation function found from the SRA data, viewed as before along the track from a viewpoint 30° to the left of it, has the somewhat remarkable form of Fig. 10b. The flight path was roughly orthogonal to the average swell direction, and it is difficult from this view alone to discern the length alongtrack of the region of high correlation. Figure 10c is a view of the autocorrelation function looking north, and Fig. 10d is an undistorted contour plot of this function. Evidently, the central peak is indeed almost conical and defines, according to our theoretical expectation, the expected instantaneous configuration of the highest waves. The long-crested oscillations with considerable spatial persistence suggest the presence of an additional discrete train of swell coming from the southeast, presumably from a distant source.

The averaged surface configurations surrounding instantaneous crests higher than 2σ (299 crests), 2.5σ (98), and 3σ (28) (Figs. 11a–c) again show a structure very close to that of the autocorrelation function. The average extreme crest configuration is again almost conical, having possibly more the nature of a standing wave formed from wave groups traveling in nearly opposite directions than of a progressive wave. Note that eyewitness reports of giant waves frequently describe them as "coming out of nowhere." (Note also that a standing wave of given energy has a maximum crest height $\sqrt{2}$ times larger than a pure progressive wave with the same energy per unit area. This is because at the point of maximum the water is instantaneously at rest, so that *all* of the kinetic energy is converted to potential energy. In a pure progressive wave, the kinetic energy of fluid elements is constant and equal to the average potential energy.)

Figure 11d shows the mean surface configuration surrounding troughs deeper than 2σ. The minimum is out of sight but extends to -1. To a helmsman in a rough sea, this may look like a black hole into which his boat might fall.

d. A fetch-limited wind sea with opposing swell (5C)

The final data were obtained about 40 minutes later at point C of Fig. 1b near buoy 44014 (CERC). The significant wave height at CERC and along the SRA track was only 2 m, so that noise was not insignificant. Directional frequency spectra from the buoy and the SRA data in Fig. 12 indicate the dominant swell of 10 sec from 140° to 150°, though the SRA spectrum may possibly resolve separate directional maxima at 130°

and 165°. This swell has propagated at oblique incidence almost through the Gulf Stream and past the shoals off Hatteras; its direction of propagation is clearly more westerly than at the other sites. The wind sea, with a period of 6–7 s, is coming almost from the north, at an angle almost 50° to the right of the local wind direction. This may be the result either of the slant-fetch effect (Donelan et al. 1985), since the available fetch immediately upwind is considerably smaller than that available to waves propagating to the right of the mean wind, or else the result of wave seeding from the mouth of the Delaware Bay, a characteristic phenomenon observed by Walsh et al. (1983) in this region but somewhat farther north.

The flight path was almost directly downwind, opposite the direction of swell propagation. The autocorrelation function in this instance is shown in Fig. 13a. Superimposed on the dominant 10-sec wave (wavelength 160 m) is a cross-track oscillation associated with the oblique 6–7 sec wind sea (wavelength about 50 m). This characteristic, as well as the overall shape, is reproduced in the mean surface configurations surrounding crests for which $\gamma = 2$ (400 of them), though the measurement noise and randomness of the wind sea begins to obscure the pattern when $\gamma = 2.5$ (124).

4. Conclusions

We believe the comparisons described here for four quite different sea states measured during SWADE provide good observational support for the simple theoretical relation (1.1) that specifies the expected spatial configuration of extreme waves as proportional to the two-dimensional spatial autocorrelation function of the wave field as a whole. That this relationship is maintained under different dynamical conditions is not surprising, since the theoretical approximation (1.1) is a statistical one for a Gaussian field and dynamics is involved only to the extent of ensuring that the wave fields under these conditions are close to Gaussian. Precisely analogous expressions should also hold for other continuous, random, Gaussian fields.

Although the extreme waves measured during this part of SWADE were hardly extreme in the sense that they would be life-threatening to a well-found ship, they were in terms of the significant wave heights in the various sea states measured. In rougher seas, the extreme waves are proportionately higher, and information on their expected configuration is probably of more direct use to a helmsman or a naval architect than is a wave spectrum. The spatial covariance, $\zeta^2 \rho(\mathbf{r})$ is of course the Fourier transform of the two-dimensional wave spectrum, and the latter is predicted routinely by wave forecast models. One final caution, though: E. Mollo-Christensen has pointed out to us and others on various occasions that wave forecast models are frequently "tuned" by comparison with pitch–roll buoy data, which may on occasion indicate a greater directional spread than is in fact present. Autocorrelation functions computed from forecast spectra may then give configurations of the type of Fig. 10 more frequently than is warranted.

Acknowledgments. This research was supported by the U.S. Office of Naval Research under Contract N00014-90-J-1623 for O.M.P. and D.G. It would clearly have been impossible without the dedicated work of the NASA staff who maintained and flew the aircraft during SWADE, the staff of the National Data Buoy Center who installed and operated the buoys, and Dr. David Wang of Computer Science Corporation who analyzed the buoy data. Dr. Lynn K. Shay kindly allowed us access to the draft of his report (1993). We are most grateful to them all.

REFERENCES

Boccotti, P., G. Barbaro, and L. Mannino, 1993: An experiment at sea on mechanics of irregular gravity waves. *J. Fluid Mech.*, in press.

Donelan, M. A., J. Hamilton, and W. H. Hui, 1985: Directional spectra of wind-generated waves. *Phil. Trans. Roy. Soc., London,* **A315,** 509–562.

Kenney, J. E., E. A. Uliana, and E. J. Walsh, 1979: The Surface Contour Radar, a unique remote sensing instrument. *IEEE Trans. Microwave Theory Tech.,* **27**(12), 1080–1092.

Longuet-Higgins, M. S., 1984: Statistical properties of wave groups in a random sea state. *Phil. Trans. Roy. Soc. London,* **A312,** 219–150.

Parsons, C. L., and E. J. Walsh, 1989: Off-nadir radar altimetry. *IEEE Trans. Geosci. Remote Sens.,* **27,** 215–224.

Phillips, O. M., D. Gu, and M. Donelan, 1993: On the expected structure of extreme waves in a Gaussian sea. 1: Theory and SWADE buoy measurements. *J. Phys. Oceanogr.,* **23,** 992–1000.

Shay, L. K., 1993: Airborne expendible current profiling during SWADE. Rosenstiel School of Marine and Atmospheric Sciences, Tech. Rep., RSMAS-93-001.

Steele, K. E., C-C. Teng, and D. W. C. Wang, 1992: Wave directional measurements using pitch-roll buoys. *Ocean Eng.,* **19,** 349–375.

Walsh, E. J., 1991: Surface contour radar directional wave spectra measurements during LEWEX. *Directional Wave Spectra,* R. C. Beal, Ed., The Johns Hopkins University Press, 86–90.

——, D. W. Hancock III, D. R. Hines, and R. N. Swift, 1983: Contamination of the fetch-limited directional wave spectrum by waves emanating from an embayment. *Proc. IGARSS '83.*

——, ——, ——, ——, and J. F. Scott, 1985a: Directional wave spectra measured with the surface contour radar. *J. Phys. Oceanogr.,* **15,** 566–592.

——, ——, ——, ——, and ——, 1985b: Elimination of directional wave spectrum contamination from noise in elevation measurements. *IEEE J. Oceanic Eng.,* **OE-11,** 376–381.